Sound transmission loss of windows on high speed trains

Yumei Zhang[1, 2], Xinbiao Xiao[1], David Thompson[2], Giacomo Squicciarini[2], Zefeng Wen [1], Zhihui Li[1], Yue Wu[1]

[1] State Key Laboratory of Traction Power, Southwest Jiaotong University, China

[2] Institute of Sound and Vibration Research, University of Southampton, UK
e-mail: zfwen@home.swjtu.edu.cn

Abstract. The window is one of the main components of the high speed train car body structure through which noise can be transmitted. To study the windows' acoustic properties, the vibration of one window of a high speed train has been measured for a running speed of 250 km/h. The corresponding interior noise and the noise in the wheel-rail area have been measured simultaneously. The experimental results show that the window vibration velocity has a similar spectral shape to the interior noise. Interior noise source identification further indicates that the window makes a contribution to the interior noise. Improvement of the window's Sound Transmission Loss (STL) can reduce the interior noise from this transmission path. An STL model of the window is built based on wave propagation and modal superposition methods. From the theoretical results, the window's STL property is studied and several factors affecting it are investigated, which provide indications for future low noise design of high speed train windows.

1. Introduction

Interior noise is one of the key parameters affecting the comfort level of high speed trains. Due to the presence of many different kinds of sources and their complex transmission paths [1, 2], the control of the interior noise of high-speed trains is quite complex. However all transmission paths to the receiver inside the cabin involve the carbody plate structures, such as the windows and extruded aluminium panels. For airborne transmission paths the sound transmission loss performance of these structures is one of the essential factors that directly affect the noise level inside the train.

The main object of the present study is the window, which is a sealed double glazed unit with air in the cavity. The sound insulation performance of double and multiple glazed windows, particularly with application to buildings has been widely studied [3-9]. The wave propagation method is one of the most effective methods. Wang et al [10], used the wave propagation method to study the insulation of an infinite double-leaf partition. Xin et al [11] applied the wave propagation method to study the sound insulation properties of finite double plate structures, and investigated the effect of the panel thickness, cavity thickness and the incidence angle. The effectiveness of this method for double plate sound insulation calculations has also been verified through comparison with experiments under different boundary conditions [12, 13].

In order to determine the importance of the window in the transmission of interior noise, the vibration acceleration characteristics of a high-speed train window and the corresponding interior noise and noise in the wheel-rail source region are first measured for a train speed of 250 km/h, which is presented in section 2. For better understanding of the window's acoustic properties, the wave propagation method is then applied in Section 3 to simulate the behaviour of a high speed train

window. In the theoretical model, several important parameters are investigated to improve further the Sound Transmission Loss (STL) according to main frequency band of the interior noise.

2. Field experimental investigation

To investigate the window's vibration properties and their effect on the interior noise, the vibration acceleration of a window of a high-speed train and the corresponding interior noise and bogie area noise have been measured simultaneously at a running speed of 250 km/h. The measured window and the interior noise test point are both located in the middle of the high speed train trailer car, as shown in figure 1(a). 15 acceleration points on the window are measured as shown in figure 1(c). To avoid adding too much mass on the window, the acceleration was measured one point at a time during steady running. Figure 1(b) shows the bogie area noise test point. The equipment used consists of a Bruel & Kjaer 4508 accelerometer (weighting 4.8 g), 4190 microphone and 8606 spherical beamforming array and using PULSE for data analysis.

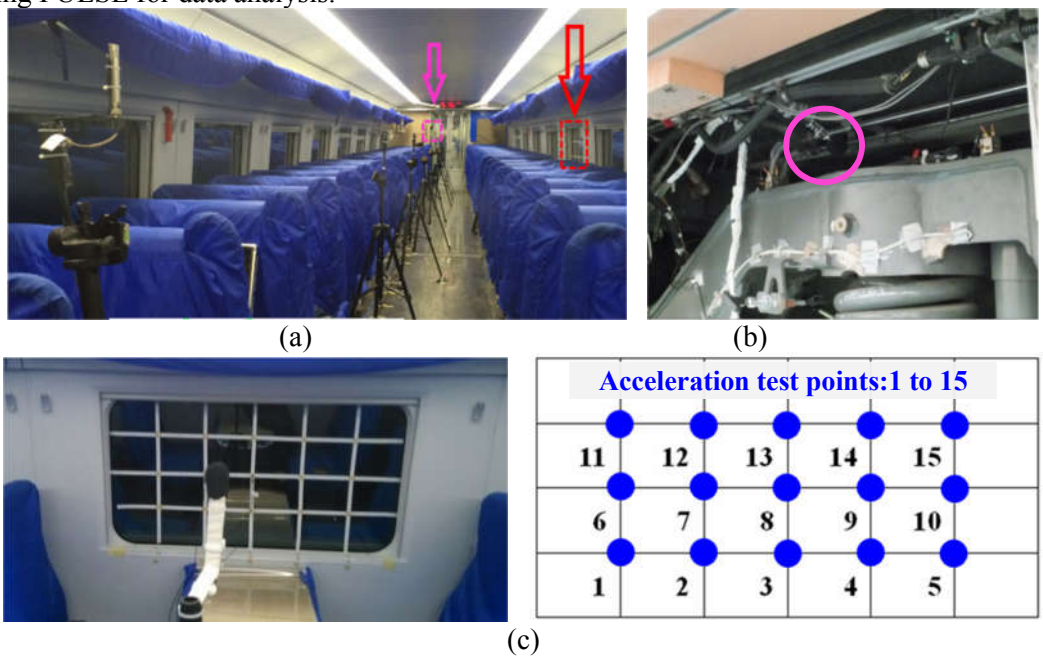

Figure 1. Photos and Schematic diagram of field test.

2.1. Interior noise and its source identification

The interior and bogie area noise test results obtained are shown in figure 2. This shows that, after A-weighting, the interior noise is dominated by the region 630~1250 Hz with its peak at the 1000 Hz frequency band. As one of the main noise sources of interior sound, the bogie area noise may shed some light on this phenomenon. It also peaks in the region 630~1250 Hz where the A-weighted level is far higher than the rest of the frequency range.

For further identification of the interior noise source, the spherical beamforming array has been used at the same interior noise test point on the coach centreline opposite the window. The source identification results are shown in figures 3(a) and 3(b). These display the sound pressure distribution (with a range of 6 dB) in the 1000 and 1250 Hz one-third octave bands respectively. In figure 3(a), the peak interior noise in the 1000 Hz band mainly comes from the two ends of the cabin, which is near the location of the bogie area and inter-coach connection. The contribution from the window is around 3 dB below the maximum contribution. At the same time, in figure 3(b), in the 1250 Hz band the interior noise mainly comes from the roof, two ends, window and floor around the centre of the cabin. Here the window is within 2 dB of the maximum contribution. On the basis of this interior noise

identification we can conclude that the window, as well as other panels from the roof and floor, has a contribution to the interior noise.

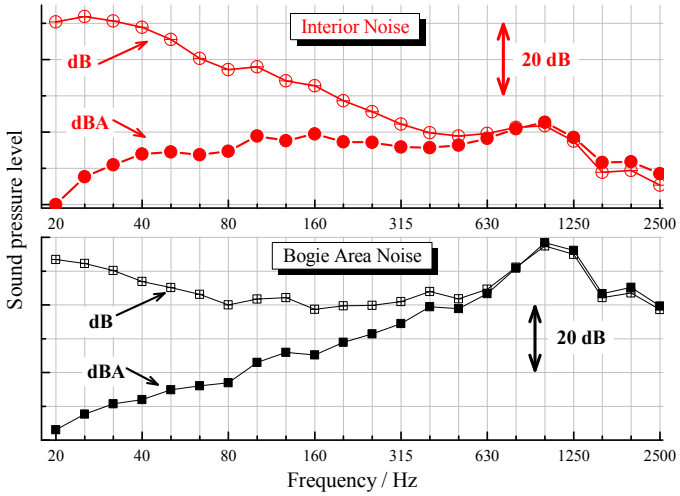

Figure 2. One-third octave band spectra of interior and bogie area noise.

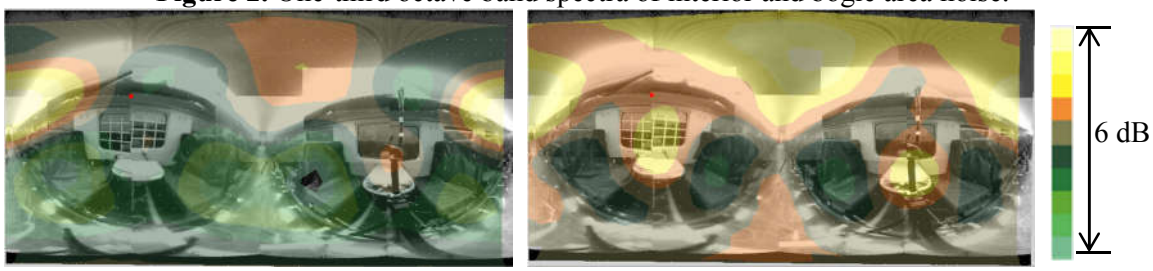

Figure 3. Interior noise source identification in one-third octave frequency bands, (a) 1000 Hz, (b) 1250 Hz.

2.2. Window's vibration

To further study the vibration property of the window and to survey its relation with the interior noise, the acceleration of the 15 points on the window has been obtained. The window's velocity is determined by integrating the acceleration and is shown in figure 4. When comparing with the unweighted interior noise level, the window's vibration velocity has a similar frequency distribution. This further supports the conclusion that the window's vibration may contribute to the interior noise.

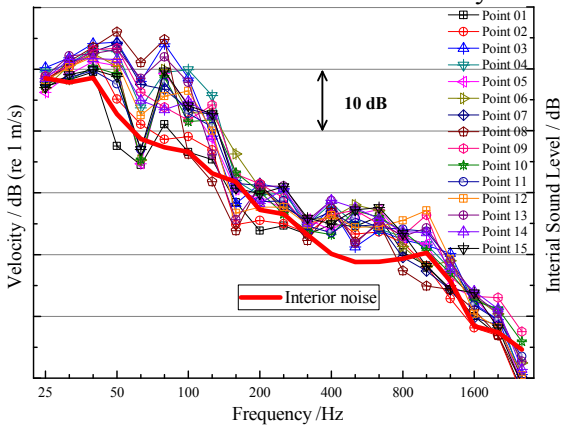

Figure 4. Comparison of window vibration velocity with interior SPL.

3. Theoretical model of window STL

Airborne sound transmission is one of the main noise contributions of a high-speed train window. To improve the acoustic properties of the window we must consider its Sound Transmission Loss (STL). In this section a theoretical STL model of a double panel with a cavity is built based on the wave propagation method and modal superposition method [12]. For simplicity, simply supported boundary conditions are used for panels. A schematic view of the window is shown in figure 5. The international standard units are used.

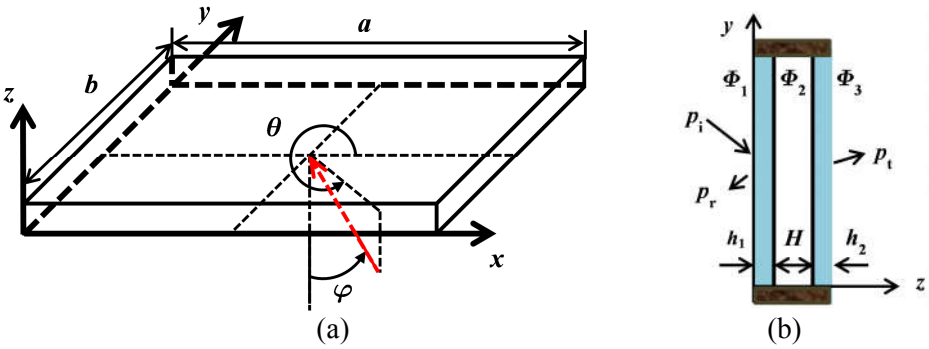

Figure 5. Schematic of sound transmission through a rectangular simply supported double panel window partition: (a) global view; (b) sectional view.

3.1. Double panel cavity model

For a plane harmonic sound wave, its acoustic potential is given by [12]:

$$\Phi(x,y,z;t) = Ie^{-j\left(k_x x+k_y y+k_z z-\omega t\right)} \tag{3.1}$$

where I is the sound amplitude; $j=\sqrt{-1}$, ω is the angular frequency, the wavenumber components are:

$$k_x = k_0 \sin\varphi\cos\theta,\ k_y = k_0 \sin\varphi\sin\theta,\ k_z = k_0\cos\varphi, k_0 = \frac{\omega}{c_0} \tag{3.2}$$

k_0 is the acoustic wavenumber in air, c_0 is the sound speed in air, and k_x, k_y, and k_z are the wavenumber components in the x, y, and z directions respectively. The equations of motion of panel 1 and panel 2 are:

$$D_1\nabla^4 w_1 + M_1\frac{\partial^2 w_1}{\partial t^2} - j\omega\rho_0(\Phi_1-\Phi_2) = 0 \tag{3.3}$$

$$D_2\nabla^4 w_2 + M_2\frac{\partial^2 w_2}{\partial t^2} - j\omega\rho_0(\Phi_2-\Phi_3) = 0 \tag{3.4}$$

where w_1 and w_2 are the displacements of the panel at the source and receiver side, respectively; ρ_0 is the air density, M_1 and M_2 are panel surface densities, D_1 and D_2 are the flexural rigidity of the panels:

$$D_i = \frac{E_i h_i^3(1+j\eta_i)}{12(1-v_i^2)} \tag{3.5}$$

The index i=1, 2 is used for the panels at the source and receiver side. E_i, h_i, η_i and v_i are the Young's modulus, thickness, damping loss factor and Poisson's ratio of panels respectively. Based on the modal superposition method, the transverse displacements of the two panels can be written as:

$$w_1(x,y,t) = \sum_{m,n}\phi_{mn}(x,y)q_{1,mn}(t), \qquad w_2(x,y,t) = \sum_{m,n}\phi_{mn}(x,y)q_{2,mn}(t) \tag{3.6}$$

m and n are the number of half-wavelengths in the x and y directions. For simply supported boundary conditions, the modal function ϕ_{mn} and modal displacements amplitude $q_{i,mn}$ can be given by:

$$\phi_{mn}(x,y) = \sin\frac{m\pi x}{a}\sin\frac{n\pi y}{b},\quad q_{1,mn}(t) = \alpha_{1,mn}e^{j\omega t},\quad q_{2,mn}(t) = \alpha_{2,mn}e^{j\omega t} \tag{3.7}$$

In the present model, there are three fluid regions, Φ_1, Φ_2, Φ_3 which represent the halfspace on the source side, the cavity between the two panels and the halfspace on the receiver side, respectively. The velocity potential for each domain can be described as the superposition of positive and negative waves in the z direction, which can be further expressed in terms of the panel modal functions as:

$$\Phi_1(x,y,z;t) = Ie^{-j\left(k_x x+k_y y+k_z z-\omega t\right)} + \beta e^{-j\left(k_x x+k_y y-k_z z-\omega t\right)} = \sum_{m,n} I_{mn}\phi_{mn}e^{-j\left(k_z z-\omega t\right)} + \sum_{m,n}\beta_{mn}\phi_{mn}e^{-j\left(-k_z z-\omega t\right)} \tag{3.8}$$

$$\Phi_2(x,y,z;t) = \varepsilon e^{-j\left(k_x x+k_y y+k_z z-\omega t\right)} + \zeta e^{-j\left(k_x x+k_y y-k_z z-\omega t\right)} = \sum_{m,n} \varepsilon_{mn}\phi_{mn}e^{-j\left(k_z z-\omega t\right)} + \sum_{m,n}\zeta_{mn}\phi_{mn}e^{-j\left(-k_z z-\omega t\right)} \tag{3.9}$$

$$\Phi_3(x,y,z;t) = \xi e^{-j\left(k_x x+k_y y+k_z z-\omega t\right)} = \sum_{m,n} \xi_{mn}\phi_{mn}e^{-j\left(k_z z-\omega t\right)} \tag{3.10}$$

where I_{mn}, β_{mn}, ε_{mn}, ζ_{mn} and ξ_{mn} can be determined by applying the orthogonal condition of the modal function by Fourier transform：

$$\lambda_{mn} = \frac{4}{ab}\int_0^b\int_0^a \lambda e^{-j\left(k_x x+k_y y\right)}\sin\frac{m\pi x}{a}\sin\frac{n\pi y}{b}dxdy \tag{3.11}$$

At the air-panel interface, the velocity compatibility equations apply:

$$z=0,\quad -\frac{\partial\Phi_1}{\partial z} = j\omega w_1,\quad -\frac{\partial\Phi_2}{\partial z} = j\omega w_1 \tag{3.12}$$

$$z=H,\quad -\frac{\partial\Phi_2}{\partial z} = j\omega w_2,\quad -\frac{\partial\Phi_3}{\partial z} = j\omega w_2 \tag{3.13}$$

Substituting equations (3.6) ~ (3.10) into equations (3.12) and (3.13), we can obtain the acoustic velocity potential parameters as a function of the panel displacements.

$$\beta_{mn} = I_{mn} - \frac{\omega\alpha_{1,mn}}{k_z},\ \varepsilon_{mn} = \frac{\omega e^{jkzH}\left(\alpha_{2,mn} - e^{jk_z H}\alpha_{1,mn}\right)}{k_z\left(1-e^{2jk_z H}\right)},\ \zeta_{mn} = \frac{\omega\left(\alpha_{2,mn}e^{jk_z H} - \alpha_{1,mn}\right)}{k_z\left(1-e^{2jk_z H}\right)},\ \xi_{mn} = \frac{\omega\alpha_{2,mn}}{e^{-jk_z H}k_z} \tag{3.14}$$

Substituting equations (3.6) ~ (3.10) and (3.14) into equations (3.3) and (3.4), the governing equation can be written in matrix form as:

$$\begin{bmatrix} A_{11} & A_{12} \\ A_{21} & A_{22} \end{bmatrix}\begin{Bmatrix} \alpha_{1,mn} \\ \alpha_{2,mn} \end{Bmatrix} = \begin{Bmatrix} F_1 \\ F_2 \end{Bmatrix} \tag{3.15}$$

where

$$A_{11} = \frac{D_1\pi^4}{a^4}m^4 + \frac{D_1\pi^4}{b^4}n^4 + 2\frac{D_1\pi^4}{a^2b^2}m^2n^2 - M_1\omega^2 - \frac{2j\omega^2\rho_0 e^{2jk_z H}}{k_z\left(1-e^{2jk_z H}\right)},\quad A_{12} = \frac{2j\omega^2\rho_0 e^{jk_z H}}{k_z\left(1-e^{2jk_z H}\right)} \tag{3.16}$$

$$A_{21} = A_{12},\quad A_{22} = \frac{D_2\pi^4}{a^4}m^4 + \frac{D_2\pi^4}{b^4}n^4 + 2\frac{D_2\pi^4}{a^2b^2}m^2n^2 - M_2\omega^2 - \frac{2j\omega^2\rho_0 e^{2jk_z H}}{k_z\left(1-e^{2jkzH}\right)} \tag{3.17}$$

$$F_1 = -2j\omega\rho_0 I_{mn},\quad F_2 = 0 \tag{3.18}$$

The terms a, b are the length and width of the window as shown in figure 5. Once the matrix is solved, the displacement amplitudes of the panels are obtained, and the velocity potential parameters in equations (3.14) can be calculated. The sound power transmission coefficient τ is a function of the elevation angle, and can be expressed as:

$$\tau(\varphi,\theta) = \frac{\sum_{m=1}^{\infty}\sum_{n=1}^{\infty}\left|\xi_{mn}\right|^2}{\sum_{m=1}^{\infty}\sum_{n=1}^{\infty}\left|I_{mn}+\beta_{mn}\right|^2} \tag{3.19}$$

φ and θ are the incident angles as defined in figure 5(a). For a diffuse incident sound field, the averaged transmission coefficient can be obtained by integration as:

$$\tau_{\text{diff}} = \frac{\int_0^{\pi/2}\int_0^{\varphi_{\text{lim}}} \tau(\varphi,\theta)\sin(\varphi)\cos(\varphi)d\theta d\varphi}{\int_0^{\pi/2}\int_0^{\varphi_{\text{lim}}} \sin(\varphi)\cos(\varphi)d\theta d\varphi} \tag{3.20}$$

where φ_{lim} is the limiting angle defining the diffuseness of the incident field. Here the limiting incident angle is 78° [12]. The sound transmission loss is given as:

$$\text{STL} = 10\log(\frac{1}{\tau}) \tag{3.21}$$

3.2. Model validation

The STL model developed here is verified by comparison with the simply supported experimental results and structural and material parameters given in [12]. According to [12], the two identical aluminium panels with length a=0.3 m, width b=0.3 m, and thickness h=1 mm are separated by an air cavity of depth H=80 mm. The STL results at normal incidence are compared in figure 6. Overall, the theoretical result has a good consistency with the measurements although there are some differences. These differences can be expected due to the deviation in the boundary conditions, material damping and so on.

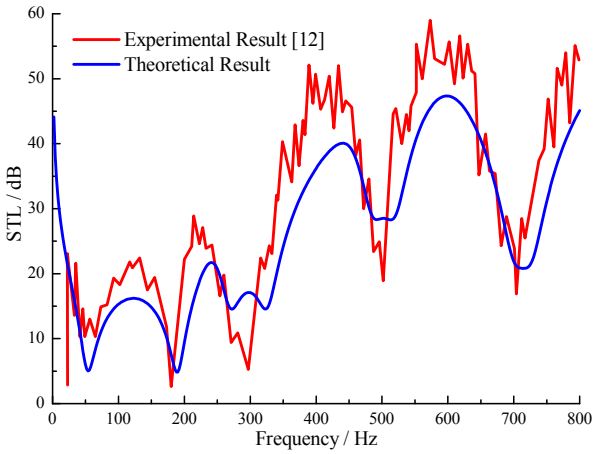

Figure 6. STL model validation.

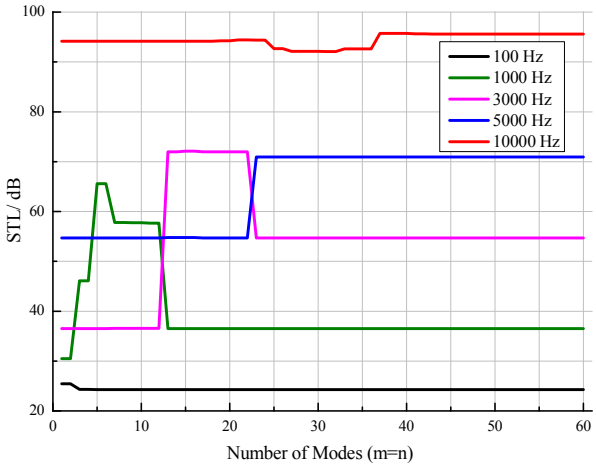

Figure 7. Convergence check of window STL.

3.3. STL property of window

The theoretical model is applied next to simulate the STL of the high-speed train window. Table 1 lists the simulation parameters of the actual window. The damping loss factor of the glass is set to 0.005. The air density ρ_0 and sound speed in air c_0 are 1.21 kg/m^3 and 343.0 m/s respectively. Due to the absorption and sealing performance at the boundary in practical windows, the air damping loss factor of the window interior cavity η_0 is defined as 0.05. The air damping is added by making the wavenumber complex, $k_0^{'} = (\omega / c_0)(1 - j\eta_0 / 2)$ in the interior cavity. The incident sound amplitude of the acoustic velocity potential, I in equation (3.8) , is fixed at 1 m^2 / s.

Table 1. Window's dimensions and material parameters

Length	**Width**	**Thickness of glass**	**Thickness of air cavity**	**Glass Young's modulus**	**Glass density**	**Glass Poisson's ratio**
a	b	h_1= h_2	H	E_1=E_2	ρ_1= ρ_2	v_1= v_2
1.4 m	0.82 m	0.005 m	0.009 m	5.5×10^{10} Pa	2500 kg/m^3	0.24

To calculate the STL of the window, the convergence of the solution is checked first. Since the vibration of the plate is calculated based on the modal superposition method, it needs to be defined how many modes are needed in the simulation. Only if enough modes are used can the convergence and accuracy of the result be assured.

As shown in figure 7, the STL at five frequencies is checked when differing numbers of modes are included in the calculation. It can be seen that when the number of modes considered in each direction is at least 40, the results at all the frequencies considered will converge. The lower the excitation frequency is, the smaller the number of modes that is needed. At 1000 Hz for example, only 15 modes in each direction would be needed. In the following results from the theoretical model, the number of modes of standard window is set to 40 in each direction.

The diffuse field STL of the window is shown in figure 8(a) and (b) in one-third octave band and narrow band forms respectively. Figure 8(a) illustrates the STL of the window from 16 to 8000 Hz. The STL generally increases with increasing frequency; at 1000 Hz for example it is 32 dB. There are four dips in the STL, which are at 20, 160, 250 and 2500-3150 Hz. For better understanding of this behaviour, the narrow band spectrum is given in figure 8(b). The frequency region can be divided into four general regions of interest, labelled as stiffness controlled, resonance controlled, mass controlled, and coincidence controlled areas [14].

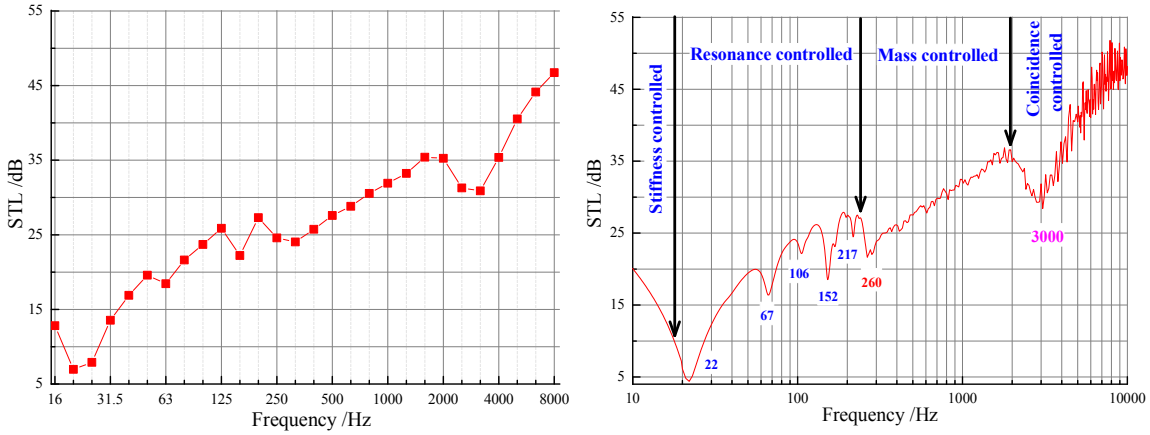

Figure 8. Diffuse field STL, (a) one third octave and (b) narrow band.

Within the frequency range plotted, seven "resonance" frequencies occur, namely 22, 67, 106, 152, 217, 260 and 3000 Hz. To identify the mechanisms of those frequencies, several typical frequencies need to be considered first. For a double panel structure, typical frequencies are the "Mass-Air-Mass" resonance, f_{MAM}, "coincidence frequency", f_{co}, and "standing wave resonance", f_{st}, which are given as follows [8].

$$f_{MAM,\varphi_0}=\frac{1}{2\pi}\sqrt{\frac{s^{'}(m_{p1}+m_{p2})}{m_{p1}m_{p2}}}=254\,\mathrm{Hz},\quad f_{MAM,\varphi}=\frac{f_{MAM,\varphi_0}}{\cos(\varphi)},\ 0\le\varphi<\frac{\pi}{2} \tag{3.22}$$

$$f_{co,\varphi_{90}}=\frac{c_0^2}{2\pi}\left\{\frac{12\rho\left(1-\nu^2\right)}{Eh^2}\right\}^{\frac{1}{2}}=2685\ \mathrm{Hz},\quad f_{co,\varphi}=\frac{f_{co,\varphi_{90}}}{\sin(\varphi)^2},\ 0<\varphi\le\frac{\pi}{2} \tag{3.23}$$

$$f_{st}=\frac{ic_0}{2H}=19058i\ \mathrm{Hz},\quad i=1,2...N \tag{3.24}$$

The parameters are the same as listed in table 1. $f_{\mathrm{MAM},\,\varphi 0}$ represents f_{MAM} at φ=0 and $f_{\mathrm{co},\,\varphi 90}$ represents f_{co} at $\varphi=\pi/2$. $s^{'}=\rho_0 c_0{}^2/H$ is the equivalent stiffness of the air in the gap. m_{p1} and m_{p2} are the mass per unit area for panel 1 and 2 respectively. The three frequencies above are all independent of the boundary conditions; although the mass-air-mass frequency can be influenced by the first bending mode of the plate the latter is sufficiently low in frequency not to influence the results in the present case.

The values of these frequencies illustrate that the dip in the diffuse field STL at 260 Hz is associated with the "Mass-Air-Mass" resonance and that at 3000 Hz belongs to the "coincidence frequency", both of which are a function of the angle of the incident sound field φ defined in figure 5. These two frequencies shed light on the dips in figure 8(a) in the 250 and 2500 Hz frequency bands. The "standing wave resonance" has its least value at 19 kHz, which is out of the frequency range considered.

The other five dips identified in the resonance controlled area of diffuse field STL are at 22, 67, 106, 152 and 217 Hz. Comparing these with the natural frequencies of the panel, listed in table 2, it can be seen that 22 Hz is mode (1, 1), 67 Hz corresponds to mode (3, 1), 106 Hz is mode (4, 1) and 152 Hz is mode (1, 3) and 217 Hz is mode (6, 1).

Table 2. First seven order natural frequencies of the radiation panel (Hz)

	n=1	**n=2**	**n=3**	**n=4**	**n=5**
m=1	**22**	71	**152**	266	413
m=2	39	88	169	283	430
m=3	**67**	115	197	311	458
m=4	**106**	155	236	350	497
m=5	156	205	286	400	547
m=6	**217**	266	348	462	608
m=7	290	339	420	535	681

To illustrate the influence of the modes in the STL, for simplicity an oblique incidence STL at 45° relative to the z axis is calculated. The modal displacement amplitude distribution of the panel on the receiver side under sound excitation at four particular frequencies, 22, 67, 106 and 152 Hz, is given in figure 9. Taking 22 Hz for example, as shown in figure 9(a), only the first mode (1, 1) dominates the response. This confirms that it is this panel resonance that leads to the dip in the STL at this frequency. Similar results are obtained for the other three frequencies although more than mode contributes. For illustration the corresponding mode shapes are shown together with the STL in figure 10.

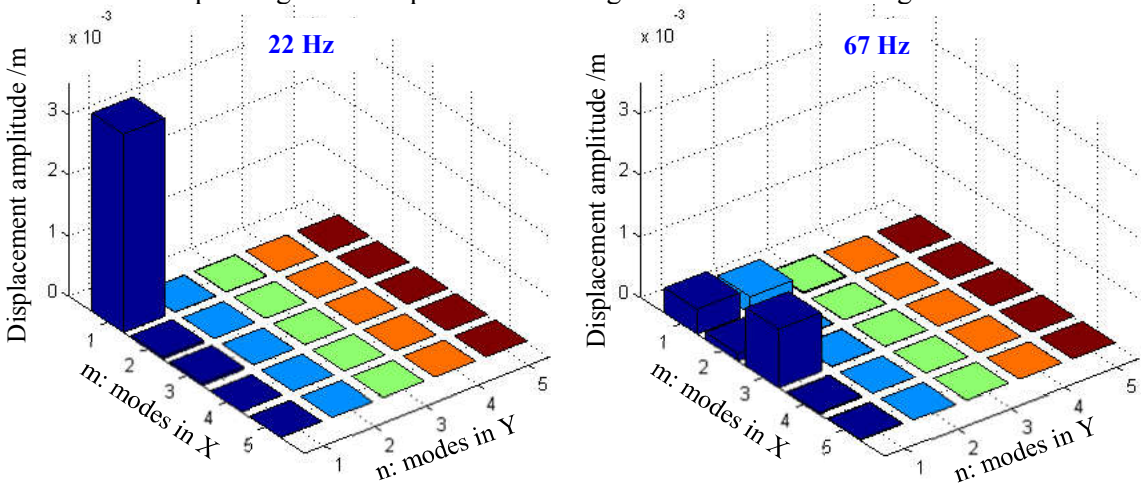

(a) **(b)**

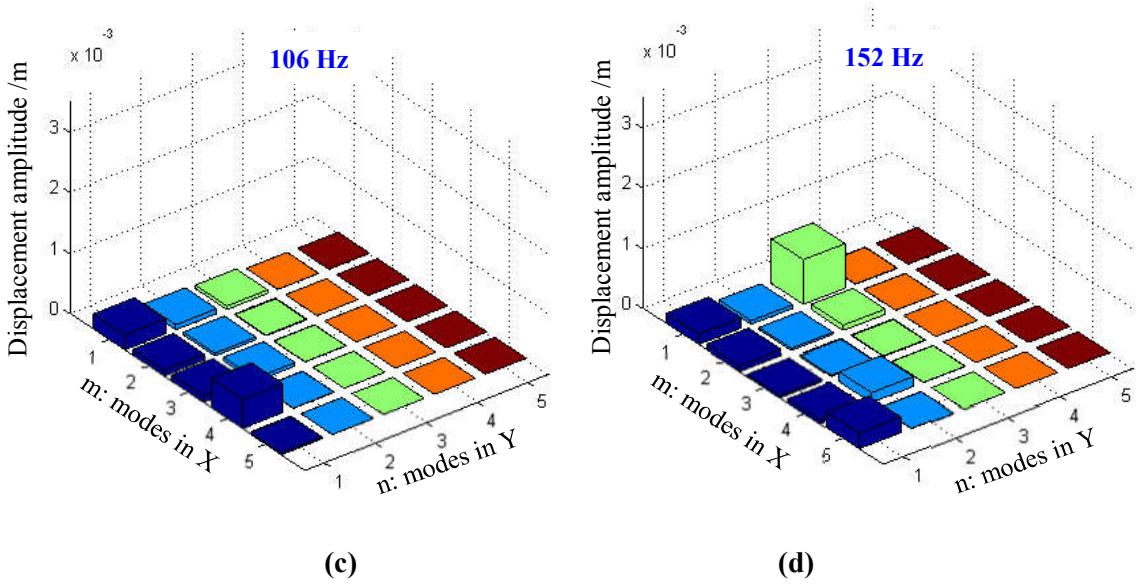

Figure 9. The displacement amplitude distribution of radiation panel under 45° oblique incident sound excitation at (a) 22 Hz, (b) 67 Hz, (c) 106 Hz, (b) 152 Hz.

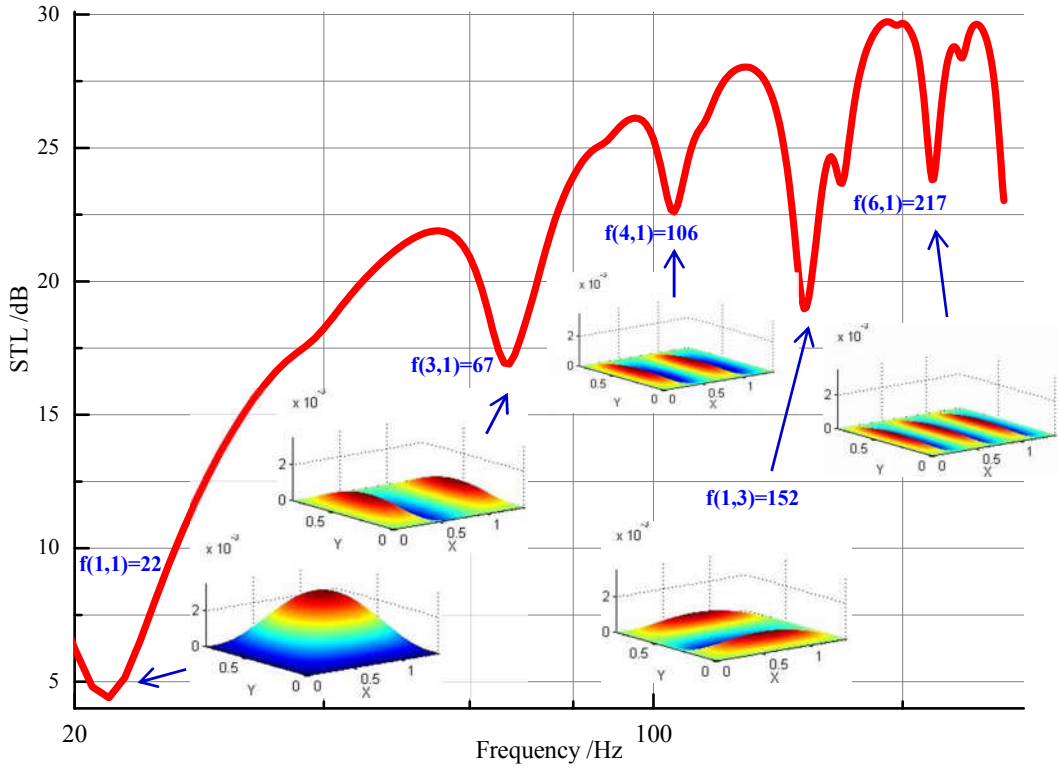

Figure 10. STL for 45° oblique plane incidence.

Compared with simply supported boundary conditions, a clamped boundary makes the panel stiffer. The first natural frequency is then found to be 42 Hz according to a finite element simulation using ANSYS. The simply supported boundary condition may not be so correct for the simulation of STL at low frequencies, especially in the stiffness-controlled and resonance areas, but the trend of the STL will still be similar. In the following parameter study, simply supported boundary conditions are again used.

3.4. Parameter study of window STL

To look for a window with a better STL, the influence of several parameters of the window is investigated. The four main structural factors studied are the air cavity thickness H, glass thickness h, window length a and damping of the interior air cavity η_0. The results are shown in figures 11, 12, 13 and 14 respectively. The parameters, h_0, H_0, a_0, b_0, are the nominal values used in the previous section, as shown in table 1. For each case the convergence was checked before performing the calculation.

Figure 11 illustrates that decreasing the air cavity gap will increase the mass-air-mass frequency, and at the same time, the STL around the 250 Hz band improves. With a larger air gap the STL around 1000~2000 Hz is increased, which is desirable because the A-weighted interior noise has a high component around 1000 Hz.

Compared with the change of air cavity gap, the STL is more sensitive to changes in the thickness of the glass over the whole frequency range. As shown in figure 12, increasing the glass thickness leads to an increase of the STL over the whole frequency range except at the first mode resonance and in coincidence region.

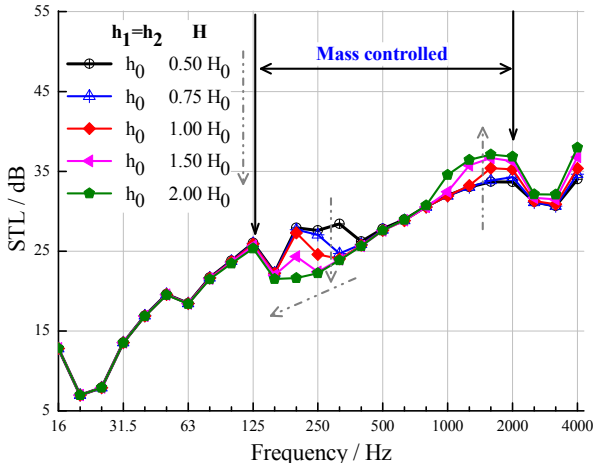

Figure 11. STL variation with cavity gap H.

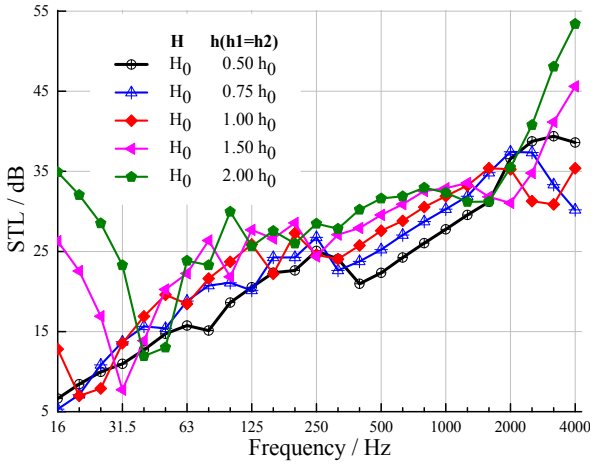

Figure 12. STL variation with glass thickness h

As shown in figure 13, the STL is sensitive to changes in the window length at low frequency in the stiffness controlled region. The first mode resonance frequency is higher when the window is shorter, giving a similar effect to the change of glass thickness, although the effect is larger. The STL in the stiffness controlled region below the first resonance is significantly increased with the shorter window. Above 250 Hz there are only small changes in the STL.

The influence of the window interior cavity damping η_0 on the STL is shown in figure 14. It can be seen that the air damping mainly influences the mass controlled area of the STL between 250 and 2000 Hz. When the air damping loss factor is increased from 0 (black line) to 0.05 (red line), the STL is increased by about 4 dB in this region. To identify why the air damping has such a great influence in this region, the STL for plane incidence at particular angles is given in figure 15. The two plots (a) and (b) are the STL for air damping of 0 and 0.05 respectively.

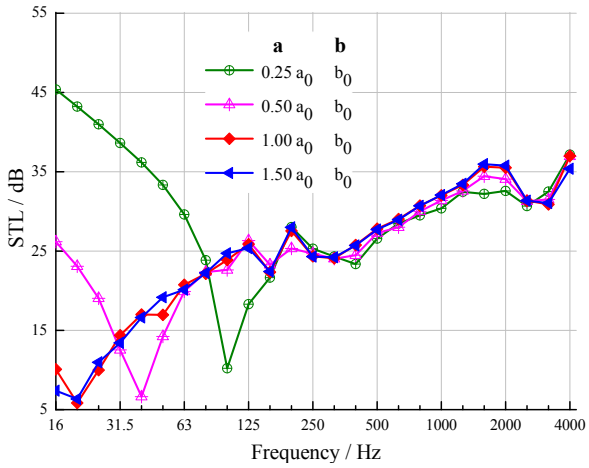

Figure 13. STL variation with length *a*.

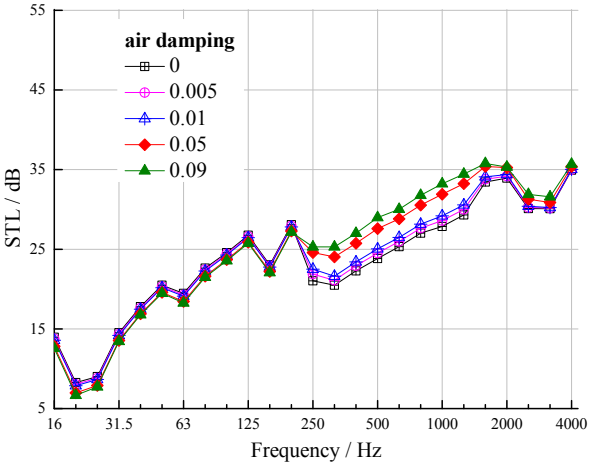

Figure 14. STL variation with air damping.

Figure 15(a) gives the STL at five incident angles. It can be seen both f_{MAM} and f_{co} vary with incident angle φ, as defined in equations (3.22)-(3.23). When φ increases from 0 to 78°, f_{MAM} increases from 254 Hz to 1222 Hz, while f_{co} decreases from infinity to 2806 Hz. In the mass controlled region, the dips in the STL at f_{MAM} from each plane incident wave have a great influence on the diffuse field STL. When adding air damping in the cavity, as figure 15(b) shows, the STL at the mass-air-mass resonance increases by more than 7 dB at each dip. The STL at the coincidence frequencies also increases, which leads to an increase of about 1 dB around the dip at 2806 Hz when φ is 78° for example. These phenomena shed some light on the effect of air damping on the diffuse field STL in figure 14.

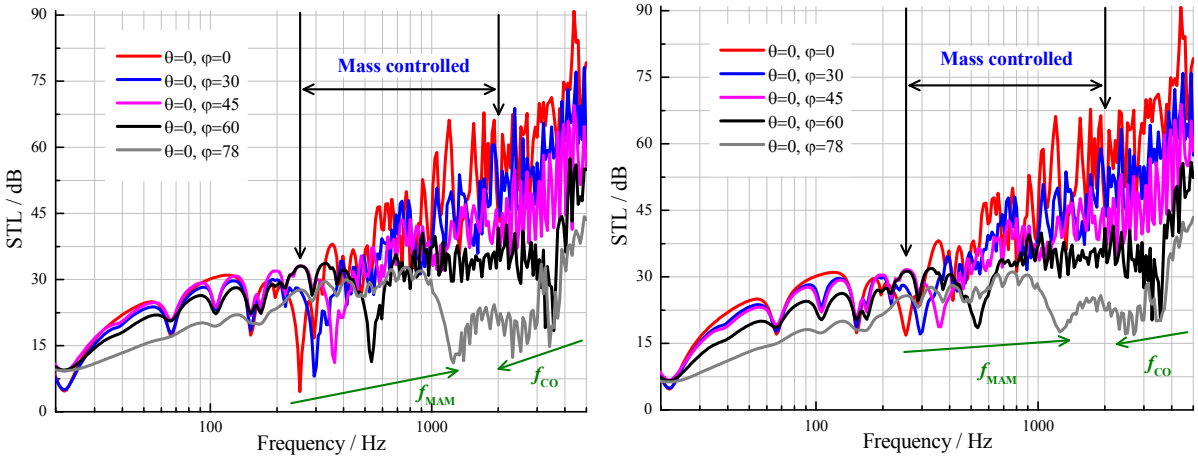

(a) **(b)**

Figure 15. Plane STL at five incident angles, air damping of window interior cavity is (a) 0, (b) 0.05.

4. Conclusion

The interior noise of a high speed train has been measured and identified at a running speed of 250 km/h. The field results show that the window is among the panel structures which contribute to the interior noise. To study and improve the STL of the window, a double panel STL model based on the wave propagation method and modal superposition method has been developed. The theoretical result shows that below 25 Hz the STL is stiffness controlled, between 25~315Hz is resonance controlled , and between 315~2500 Hz is mass controlled. The main interior A-weighted noise has its peak in the mass controlled frequency region, in which increasing the thickness of the glass provides the most significant improvement in STL. Increasing the air gap and damping also has some benefit.

In practice, the interior noise level and its dominant frequencies vary with many factors, including the running speed. Even at a fixed running speed, the interior noise frequency distribution will vary from one cabin to another and also spatially within the single cabin. The window can be designed more specifically for particular locations in the train, and the present work can provide a reference for its low noise design.

Extruded panels are also a major interior sound transmission path as identified in this work. Further research concerning these paths will be carried out in the future work.

Acknowledgements

The present work is supported by the National Natural Science Foundation of China (Nos. U1434201, 51475390) and the Research Foundation of the state key laboratory of traction power of China (No. 2015TPL_T08). We are also grateful for the funding of China Scholarship Council (CSC) which supports Yumei Zhang's visiting study at University of Southampton.

References

[1] David Thompson 2009 *Railway Noise and Vibration, 1st Edition Mechanisms, Modelling and Means of Control* (Oxford, Elsevier Science) chapter 14 pp 465–483

[2] Jie Zhang, Guang-Xu Han, Xin-Biao Xiao, Rui-Qian Wang, Yue Zhao, Xue-Song Jin 2014 Influence of wheel polygonal wear on interior noise of high-speed trains, *Journal of Zhejiang University-SCIENCE A (Applied Physics & Engineering)*. 15(12):1002-1018.

[3] Carl Hopkins 2007 *Sound Insulation* (Oxford, Elsevier Science) chapter 4 pp 418–509

[4] Qibo Mao, Stanislaw Pietrzko 2010 Experimental study for control of sound transmission through double glazed window using optimally tuned Helmholtz resonators. *Applied Acoustics*. 71(1): p. 32-38.

[5] Kamal Idrisi, Marty E. Johnson, Alessandro Toso and James P. Carneal 2009 Increase in transmission loss of a double panel system by addition of mass inclusions to a poro-elastic layer: A comparison between theory and experiment. *Journal of Sound and Vibratio*n. 323(1–2): p. 51-66.

[6] A. Tadeu, A. Pereira, L. Godinho and J. Antonio 2007 Prediction of airborne sound and impact sound insulation provided by single and multilayer systems using analytical expressions. *Applied Acoustics*. 68(1): p. 17-42.

[7] Pellicier, A. and N. Trompette 2007 A review of analytical methods, based on the wave approach, to compute partitions transmission loss. *Applied Acoustics*. 68(10): p. 1192-1212.

[8] James P. Carneal, and Chris R. Fuller 2004 An analytical and experimental investigation of active structural acoustic control of noise transmission through double panel systems. *Journal of Sound and Vibration*. 272(3–5): p. 749-771.

[9] O. E. Kaiser, S.J. Pietrzko, and M. Morari 2003 Feedback control of sound transmission through a double glazed window. *Journal of Sound and Vibration*. 263(4): p. 775-795.

[10] J. Wang, T. J. Lu, J. Woodhouse, R.S. Langley and J. Evans, 2005 Sound transmission through lightweight double-leaf partitions theoretical modelling. *Journal of Sound and Vibration*

[11] F. X. Xin, T. J. Lu and C. Q. Chen 2008 Vibroacoustic behavior of clamp mounted double-panel partition with enclosure air cavity. *J. Acoust. Soc. Am*. 124(6).

[12] F. X. Xin and T. J. Lu 2009 Analytical and experimental investigation on transmission loss of clamped double panels Implication of boundary effects. *J. Acoust. Soc. Am*. 125 (3).

[13] Tianjian Lu and Fengxian Xin 2014 *Vibro-Acoustics of Lightweight Sandwich Structures* (Beijing, Since Press) chapter 1 pp 1–12

[14] Frank Fahy and David Thompson 2014 *Fundamentals of Sound and Vibration, Second Edition* (Boca Raton, FL: CRC Press) chapter 5 pp 236–257